Inorg. Chem. **2006**, *45*, 7600–7611

Electronic Structures and Absorption Spectra of Linkage Isomers of Trithiocyanato (4,4′,4′′-Tricarboxy-2,2′:6,2′′-terpyridine) Ruthenium(II) Complexes: A DFT Study

Sutapa Ghosh, G. Krishna Chaitanya, and K. Bhanuprakash*

Inorganic Chemistry Division, Indian Institute of Chemical Technology, Hyderabad-500 007, India

Md. K. Nazeeruddin and M. Grätzel

Laboratory for Photonics and Interfaces, Institute for Physical Chemistry, Swiss Federal Institute of Technology, CH-1015 Lausanne, Switzerland

P. Yella Reddy

Aisin Cosmos R&D Company, Hyderabad-500 007, India

Received October 26, 2005

Black dye (BD), isomer **1** ($[Ru^{II}(H_3\text{-tctpy})(NCS)_3]^{-1}$, where H_3-tctpy = 4,4′,4′′-tricarboxy-2,2′:6,2′′-terpyridine) is known to be an excellent sensitizer for dye-sensitized solar cells and exhibits a very good near-IR photo response, compared to other ruthenium dyes. Because isothiocyanate is a linear ambidentate ligand, BD has three other linkage isomers, $[Ru(H_3\text{-tctpy})(NCS)_2(SCN)]^{-1}$, isomer **2** and **2′**, and $[Ru(H_3\text{-tctpy}))(SCN)_3]^{-1}$, isomer **3**. In this study, we have calculated the geometry of BD and its isomers by DFT. Further, we have analyzed the bonding in these isomers using NBO methods. TDDFT calculations combined with scalar relativistic zero-order regular approximations (SR-ZORA) have been carried out to simulate the absorption spectra. Calculations have been performed for the isomers both in vacuo and in solvent (ethanol). The inclusion of the solvent is found to be important to obtain spectra in good agreement with the experiment. The first absorption bands are dominated by the metal-to-ligand charge transfer (MLCT) and ligand-to-ligand charge transfer (LLCT).

Introduction

Polypyridine complexes of transition metal ions are important because of their photophysical and photochemical properties.[1−3] These complexes, as photosensitizers in model systems, play important roles in fields related to solar energy conversion, the storage of light, and electronic information.[4−8] 2,2′-Bipyridine (bpy) complexes of transition metals, $M(bpy)^{+2}$ (M= Ru, Os), are one of the most-studied metal-containing species in the last two decades.[9−10] But only a few photophysical reports have been devoted to terpyridine (tpy), $M(tpy)^{+2}$ analogues, because $M(tpy)^{+2}$ exhibits less-favorable photophysical properties (lack of luminescence and a very short excited-state lifetime at room temperature) than $M(bpy)^{+2}$. The structures of $M(tpy)^{+2}$, however, have many more advantages than that of $M(bpy)^{+2}$: first, $M(tpy)^{+2}$

* To whom correspondence should be addressed. E-Mail: bhanu2505@yahoo.co.in.

(1) Zhou, X.; Ren, A.-M.; Feng, J.-K. *J. Organomet. Chem.* **2005**, *690*, 338.
(2) Nazeeruddin, M. K.; Kay. A.; Rodicio, I.; Humphry-Baker, R.; Muller, E.; Liska, P.; Vlachopoulos, N.; Grätzel, M. *J. Am. Chem. Soc.* **1993**, *115*, 6382.
(3) Yang, L.; Ren, A.-M.; Feng, J.-K.; Liu, X.-D.; Ma, Y.-G.; Zhang, H.-X. *Inorg. Chem.* **2004**, *43*, 5961.
(4) Balzani, V.; Juris, A.; Venturi, M.; Campagna, S.; Serroni, S. *Chem. Rev.* **1996**, *96*, 956.
(5) Barigelletti, F.; Flamigni, L. *Chem. Soc. Rev.* **2000**, 1.
(6) Sun, L.; Hammarstrom, L.; Akemark. B; Styring. S. *Chem. Soc. Rev.* **2001**, 36.
(7) Ballardini, R.; Balzani, V.; Credi, A.; Gandolfi, M. T.; Venturi. M. *Acc. Chem. Res.* **2001**, *34*, 445.
(8) (a) Pomeranc, D.; Heitz, V.; Chamborn, J. C.; Sauvage, J. P. *J. Am. Chem. Soc.* **2001**, *123*, 12215. (b) Juris, A.; Balzani, V.; Barigelletti, F.; Campagna, S.; Belser, P.; von Zelewsky, A. *Coord. Chem. Rev.* **1988**, *84*, 85.
(9) De Armond, M. K.; Myrick, L. M. *Acc. Chem. Res.* **1989**, *22*, 364.
(10) Zhao, W.; Hou, Y. J.; Wang, X. S.; Zhang, B. W.; Cao, Y.; Yang, R.; Wang, W. B.; Xiao, X. R. *Sol. Energy Mater. Sol. Cells* **1999**, *58*, 173.

10.1021/ic051851g CCC: $33.50
Published on Web 08/25/2006

complexes are achiral, contrary to mixtures of facial and meridional isomers and two enantiomers, and second, two substituents on $M(bpy)^{+2}$ complexes can give rise to triads with cis-type geometrical arrangements, without the possibility of control, whereas substituents in the 4′ positions of $M(tpy)^{+2}$ lead to triads where the two substituents lie opposite with respect to the photosensitizer.[8] With the development of supramolecular chemistry, there has been a growing interest in Ru(II) tpy complexes. There are many reports on the photophysical properties of Ru complexes, and it is now known that there are three important factors which can tune the photophysical properties of a complex: (1) the nature of the central metal ion, (2) the nature of the acceptor ligand (e.g., bpy, tpy, etc.), and (3) the presence of a donor ligand, which can influence charge-transfer processes.[11−13]

Recently, a black dye, tri(thiocyanato)-(4,4′,4″-tricarboxy-2,2′:6,2″-terpyridine) Ru(II) (BD), has been found to have better near-IR photo response than other Ru dyes[11,14.] Because it is a linear ambidentate ligand, thiocyanate has three linkage isomers.[15] An understanding of the different linkage isomers of a particular dye can be a very interesting and exciting approach for tuning of the spectral properties of metal complexes. The donor units of the ligand can tune the metal t_{2g} orbital energies, and the acceptor units can tune the π^* molecular orbitals. Experimental results of BD show that the UV−vis spectra of the three isomers are dominated by metal-to-ligand charge-transfer transitions (MLCT) in the visible region.[14−15] An ethanolic solution of the three isomers of BD show lowest MLCT maxima at 620, 590, and 570 nm, respectively, and the λ_{max} of the low-energy MLCT band of one isomer is red shifted 50 nm compared to another isomer .[15] Such shifts are usually interpreted in terms of the different solvation interactions between the polar groups bound to the metal center and the solvent, and these mainly depend on the solvent polarity and hydrogen bond.

The coordination sites can be used to finely tune the spectral properties and stabilize the hole that is being generated on the metal, after an electron is injected into the conduction band. An understanding of the photochemistry of the transition metal complexes requires knowledge of the properties of molecular orbitals, spectra, and appropriate excited states. These spectroscopic and structural features are a big challenge to the interplay between theory and experiment and have important implications for the spectroscopy and photochemistry of the broad and important class of low-valent metal complexes containing electron-donating substituents. Moreover, their photochemistry and photophysics represent a challenge to the understanding of excited-state dynamics. The major difficulties in the selection of a reliable computational approach come from the size of such systems and the presence of strong electron correlation effects. The latter problems are difficult to treat in the framework of the quantum mechanical methods rooted in the Hatree−Fock (HF) theory. As a matter of fact, the post-Hartree−Fock methods that are needed to obtain reliable excited-state properties have scaling properties (in time) with the number of electrons (N6 or worse) which prevent their application to large systems.[16] On the other hand, density functional theory (DFT) has been remarkably successful at providing a means to evaluate a variety of ground-state properties with an accuracy close to that of post-HF methods.[17,18] As a consequence, there is currently a great interest in extending DFT calculations to excited electronic states.[19] In this context, the time-dependent DFT approach (TDDFT) offers a rigorous route to the calculation of vertical electronic excitation spectra.[20−22]

In contrast to the numerous experimental results, so far only one theoretical investigation, limited to the gas phase, has been performed[13] to study the electronic structure of BD. Moreover, no detailed study of the bonding in its isomers and the effect of solvent on the excitation of these isomers has been performed. This investigation focuses on the comparative study of ground-state properties, such as energies, geometries, and population analysis in molecular orbitals, of BD and its isomers by different DFT methods including scalar relativistic ZORA. This investigation also focuses on NBO analysis and the absorption spectra of these three isomers. Further calculations are performed in ethanol solvents, and the results in the gas phase and in ethanol are compared to study solvent effects. The experimental information coupled with DFT calculations is shown to yield a comprehensive understanding of the electronic structure of these complexes. In this work, we show that with a reasonable computational effort, TD-DFT can reproduce the spectroscopic properties of the BD and its other linkage isomers well.

Computational Details

DFT calculations of the electronic ground state of the four linkage isomers of BD have been carried out using both Gaussian 03W (G03W)[23] and Amsterdam Density Functional (ADF2005.01b)[24] packages. It has been found that the mPW (mPWx + PW91c) parametrization gives good results for Ru(II) metal complexes.[25] Thus, the mPW method has been used for calculations on the electronic states of four isomers, in which the combination of the Perdew−Wang 1991 exchange functional and modified by Adamo and Barone (mPWx) with the Perdew and Wang's 1991 gradient-corrected correlation functional (PW91c)[26] has been constructed. A mixed basis set has been used in G03w for geometry optimization [LANL2DZ, (double-ξ quality) which uses Dunning D95V basis

(11) Nazeerudin, M. K.; Pechy, P.; Renouard, T.; Zakeeruddin, S. M.; Humphry-Baker, R.; Comte, P.; Liska, P.; Cevey, L.; Costa, E.; Shklover, V.; Spiccia, L.; Deacon, G. B.; Bignozzi, C. A.; Grätzel, M. *J. Am. Chem. Soc.* **2001**, *123*, 1613.
(12) Aiga, F.; Tada, T. *Sol. Energy Mater. Sol. Cells* **2005**, *85*, 437.
(13) Aiga, F.; Tada, T. *J. Mol. Struct.* **2003**, *658*, 25.
(14) Nazeerudin, M. K.; Pechy, P.; Grätzel, M. *Chem. Commun.* **1997**, 1705.
(15) Nazeerudin, M. K.; Grätzel, M. *J. Photochem. Photobiol. A* **2001**, *145*, 79.
(16) Guillemoles, J. F.; Barone, V.; Joubert, L.; Adamo, C. *J. Phys. Chem. A* **2002**, *106*, 11354.
(17) Koch, W.; Holthausen, M. C. *A Chemist's Guide to Density Functional Theory*; Wiley-VCH: Weinheim, Germany, 2000.
(18) Adamo, C.; di Matteo, B. V. *Adv. Quantum Chem.* **1999**, *36*, 4.
(19) Lee, C.; Yang, W.; Parr, R. G. *Phys Rev. B.* **1998**, *37*, 785.
(20) Bauernschmitt, R.; Ahlrichs, R. *Chem. Phys. Lett.* **1996**, *256*, 454.
(21) Casida, M. E.; Jamorski, C.; Casida, K. C.; Salahub, D. R. *J. Chem. Phys.* **1998**, *108*, 4439.
(22) Matsuzawa, N. N.; Ishitani, A.; Dixon, D. A.; Uda, T. *J. Phys. Chem. A* **2001**, *105*, 4953.

functions on first row atoms,[27] Los Alamos, ECP plus DZ on Na−Bi[28] basis set on Ru, and 6-31G(d,p)[29] basis functions on H, C, N, O, and S]. Within the ADF program, geometry optimizations are performed using the standard ADF IV basis set, which is an uncontracted triple-STO basis set, with a triple-nd, $(n + 1)$s basis with one $(n + 1)$p function, for all atoms.[30] The cores (1s for C and O, 1s−2p for S, and 1s−3d for Ru) are kept frozen. Scalar relativistic effects are accounted for using the scalar zero-order regular approximation, SR-ZORA.[33,34]

The excitation energies and oscillator strengths for the four isomers at the optimized geometry in the ground state are obtained in the framework of TDDFT calculations with the same basis sets as that for the ground state using the ADF software. We have used the Vosko−Wilk−Nusair LDA parametrization[35] and the adiabatic local density approximation (ALDA) for the XC kernel, in the post-SCF step. To incorporate the asymptotic correction, the van Leeuwen−Baerends functional (LB94)[38] has also been combined as gradient correction in the SCF step. In the LB94 functional, the exchange correlation potential is computed from the exact charge density. We have also included SR-ZORA in this study. In combination with TDDFT, scaled orbital energies are used as default. The calculated absorption spectrum of the Ru(II) complexes is very sensitive the solvent effects;[16,39] hence TDDFT calculations in solvent (ethanol) are also carried out, in addition to calculations in the gas phase. The conductor like screening model (COSMO)[40] has been used to simulate the solvation effects as implemented in the ADF code,[41] using the optimized structures in gas phase. The COSMO model is a dielectric model in which the solute molecule is embedded in a molecule-shaped cavity surrounded by a dielectric medium with given dielectric constant, ϵ. Energy-related terms are computed for a conductor first, then scaled by the function

$$f(\epsilon) = (\epsilon - 1)/(\epsilon + x) \quad (1)$$

where x is the empirical scaling factor.

Results and Discussion

(a) Molecular Structure and NBO Analysis. Molecular structures of isomers **1**, **2**, **2′**, and **3** (Figure 1) in the gas phase, optimized by different methods and basis sets using both the G03W and ADF packages, are summarized in Table 1. Only selected bond lengths and angles are shown here, and for comparison, the crystal data of isomer **1** obtained from literature is also given.[42] Ru(II) has a 4d valence shell which is more spatially extended than metals with a 3d valence shell. Thus, Ru(II) tends to form low-spin complexes[43] because of the large ligand field splitting; therefore, the ground states of $[Ru(H_2O)]_6^{+2}$ and $Ru(NH_3)_6^{+2}$ are considered to be singlets.[44] In this paper, only the lowest-singlet states of BD and its other linkage isomers are investigated. In all calculations reported in this paper, we considered the three carboxylic groups of four linkage isomers of trithiocyanato(4,4′,4″-tricarboxy-2,2′:6,2″-terpyridine) Ru(II) complexes to be protonated, which represents the complex at pH <7.

In its +2 oxidation state, the Ru atom adopts a low-spin $4d^6 5s^0$ electronic configuration, in which three d orbitals are doubly occupied and two s orbitals are empty. Because of this, the complexes investigated display a pseudo-octahedral arrangement of ligands around the metal atom in the optimized structure. The lowest-optimized geometry of isomer **1** is a C_S symmetry, and the lowest-optimized geometries of the other isomers are in C_1 symmetry. The tpy ligand is coordinated to Ru(II) through nitrogen, and the three pyridine rings of tpy occupy three "equatorial" positions

(23) Frisch, M. J.; Trucks, G. W.; Schlegel, H. B.; Scuseria, G. E.; Robb, M. A.; Cheeseman, J. R.; Montgomery, J. A., Jr.; Vreven, T.; Kudin, K. N.; Burant, J. C.; Millam, J. M.; Iyengar, S. S.; Tomasi, J.; Barone, V.; Mennucci, B.; Cossi, M.; Scalmani, G.; Rega, N.; Petersson, G. A.; Nakatsuji, H.; Hada, M.; Ehara, M.; Toyota, K.; Fukuda, R.; Hasegawa, J.; Ishida, M.; Nakajima, T.; Honda, Y.; Kitao, O.; Nakai, H.; Klene, M.; Li, X.; Knox, J. E.; Hratchian, H. P.; Cross, J. B.; Bakken, V.; Adamo, C.; Jaramillo, J.; Gomperts, R.; Stratmann, R. E.; Yazyev, O.; Austin, A. J.; Cammi, R.; Pomelli, C.; Ochterski, J. W.; Ayala, P. Y.; Morokuma, K.; Voth, G. A.; Salvador, P.; Dannenberg, J. J.; Zakrzewski, V. G.; Dapprich, S.; Daniels, A. D.; Strain, M. C.; Farkas, O.; Malick, D. K.; Rabuck, A. D.; Raghavachari, K.; Foresman, J. B.; Ortiz, J. V.; Cui, Q.; Baboul, A. G.; Clifford, S.; Cioslowski, J.; Stefanov, B. B.; Liu, G.; Liashenko, A.; Piskorz, P.; Komaromi, I.; Martin, R. L.; Fox, D. J.; Keith, T.; Al-Laham, M. A.; Peng, C. Y.; Nanayakkara, A.; Challacombe, M.; Gill, P. M. W.; Johnson, B.; Chen, W.; Wong, M. W.; Gonzalez, C.; Pople, J. A. *Gaussian 03*, revision 01; Gaussian, Inc.: Wallingford, CT, 2004.

(24) (a) Te Velde, G.; Bickelhaupt, F. M.; van Gisbergen, S. J. A.; Fonseca Guerra, C.; Baerends, E. J.; Snidjers, J. G.; Ziegler, T. *J. Comput. Chem.* **2001**, *22*, 931. (b)Fonseca Guerra, C.; Snidjers, J. G.; Te Velde, G.; Baerends, E. *J. Theor. Chem. Acc.* **1998**, *99*, 391. (c) *Vrije ADF 2004.01*; SCM: Amsterdam, 2004.

(25) Pourtois, G.; Beljonne, D.; Moucheron, C.; Schumm, S.; Kirsch-De Mesmaeker, A.; Lazzaroni, R.; Bredas, J.-L. *J. Am. Chem. Soc.* **2004**, *126*, 683.

(26) Adamo, C.; Barone, V. *J. Chem. Phys.* **1998**, *108*, 664.

(27) Dunning, T. H., Jr.; Hay, P. J. In *Modern Theoretical Chemistry*; Miller, W. H., Ed.; Plenum: New York, 1976; p 1.

(28) (a) Hay, P. J.; Wadt, W. R. *J. Chem. Phys.* **1985**, *82*, 270. (b) Wadt, W. R.; Hay, P. J. *J. Chem. Phys.* **1985**, *82*, 284. (c) Hay, P. J.; Wadt, W. R. *J. Chem. Phys.* **1985**, *82*, 299.

(29) Ditchfield, R.; Hehre, W. J.; Pople, J. A. *J. Chem. Phys.* **1971**, *54*, 724.

(30) Baerends, E. J.; Ellis, D. E.; Ros, P. *Chem. Phys.* **1973**, *2*, 41.

(31) Adamo, C.; Barone, V. *J. Chem. Phys.* **1998**, *108*, 664.

(32) Perdew, J. P.; Chevary, J. A.; Vosko, S. H.; Jackson, K. A.; Pederson, M. R.; Singh, D. J.; Fiolhais, C. *Phys. Rev. B* **1992**, *46*, 6671.

(33) (a) Snijders, J. G.; Baerends, E. J. *Mol. Phys.* **1978**, *36*, 1789. (b) Snijders, J. G.; Baerends, E. J.; Ros, P. *Mol. Phys.* **1979**, *38*, 1909. (c) Ziegler, T.; Snijders, J. G.; Baerends, E. J. *J. Chem. Phys.* **1981**, *74*, 1271.

(34) (a) van Lenthe, E.; Snijders, J. G.; Baerends, E. J. *J. Chem. Phys.* **1996**, *105* (15), 6505. (b) van Lenthe, E.; van Leeuwen, R.; Baerends, E. J.; Snijders, J. G. *Int. J. Quantum Chem.* **1996**, *57*, 281. (c) Rosa, A.; Baerends, E. J.; van Gisbergen, S. J. A.; van Lenthe, E.; Groeneveld, J. A.; Snijders, J. G. *J. Am. Chem. Soc.* **1999**, *121*, 10356.

(35) Vosko, S. H.; Wilk, L.; Nusair, M. *Can. J. Phys.* **1980**, *58*, 1200.

(36) Becke, A. D. *Phys. Rev. A* **1988**, *38*, 3098.

(37) Perdew, J. P.; Wang, Y. *Phys. Rev. B* **1986**, *33* (12), 8822.

(38) Leeuwen, R. V.; Baerends, E. J. *Phys. Rev. A* **1994**, *49* (4), 2421.

(39) (a) Fantacci, S.; De Angelis, F.; Sgamellotti, A.; Re, N. *Chem. Phys. Lett.* **2004**, *396*, 43. (b) Joubert, L.; Guillemoles, J. F.; Adamo, C.; *Chem. Phys. Lett.* **2003**, *371*, 378. (c) Angelis, F. D.; Fantacci, S.; Selloni, A.; Nazeeruddin, M. K. *Chem. Phys. Lett.* **2005**, *415*, 115. (d) Nazeeruddin, M. K.; Angelis, F. D.; Fantacci, S.; Selloni, A.; Viscardi, G.; Liska, P.; Ito, S.; Takeru, B.; Grätzel, M. *J. Am. Chem. Soc.* **2005**, *127*, 16835. (e) Fantacci, S.; Angelis, F. D.; Selloni, A. *J. Am. Chem. Soc.* **2003**, *125*, 4381. (f) Batista, E. R.; Martin, R. L. *J. Phys. Chem. A* **2005**, *109*, 3128. (g) Labat, F.; Laine, P. P.; Ciofini, I.; Adamo. C. *Chem. Phys. Lett.* **2006**, *417*, 445. (h) Angelis, F. D.; Fantacci, S.; Selloni, A. *Chem. Phys. Lett.* **2004**, *389*, 204. (i) Pollard, J. A.; Zhang, D.; Downing, J. A.; Knorr, F. J.; McHale, J. L. *J. Phys. Chem. A* **2005**, *109*, 11443.

(40) (a) Klamt, A.; Schüürmann, G. *J. Chem. Soc., Perkin Trans.* **1993**, *2*, 799. (b) Klamt, A. *J. Phys. Chem.* **1995**, *99*, 2224. (c) Klamt, A.; Jones, V. *J. Chem. Phys.* **1996**, *105*, 9972.

(41) Pye, C. C.; Ziegler, T. *Theor. Chem. Acc.* **1999**, *101*, 396.

(42) Shklover, V.; Nazeeruddin, M. K.; Grätzel, M.; Ovchinnikov, Yu. E. *Appl. Organomet. Chem.* **2003**, *16*, 635.

(43) Akesson, R.; Pettrtson, L. G. M.; Sandstrom, M.; Wahlgren, J. *J. Am. Chem. Soc.* **1994**, *116*, 8691.

(44) Perez, W. J.; Lake, C. H.; See, R. F.; Toomey, L. M.; Churchill, M. R.; Takeuchi, K. J.; Radano, C. P.; Boyko, W. J.; Bessel, C. A. *J. Chem. Soc., Dalton Trans.* **1999**, 2281.

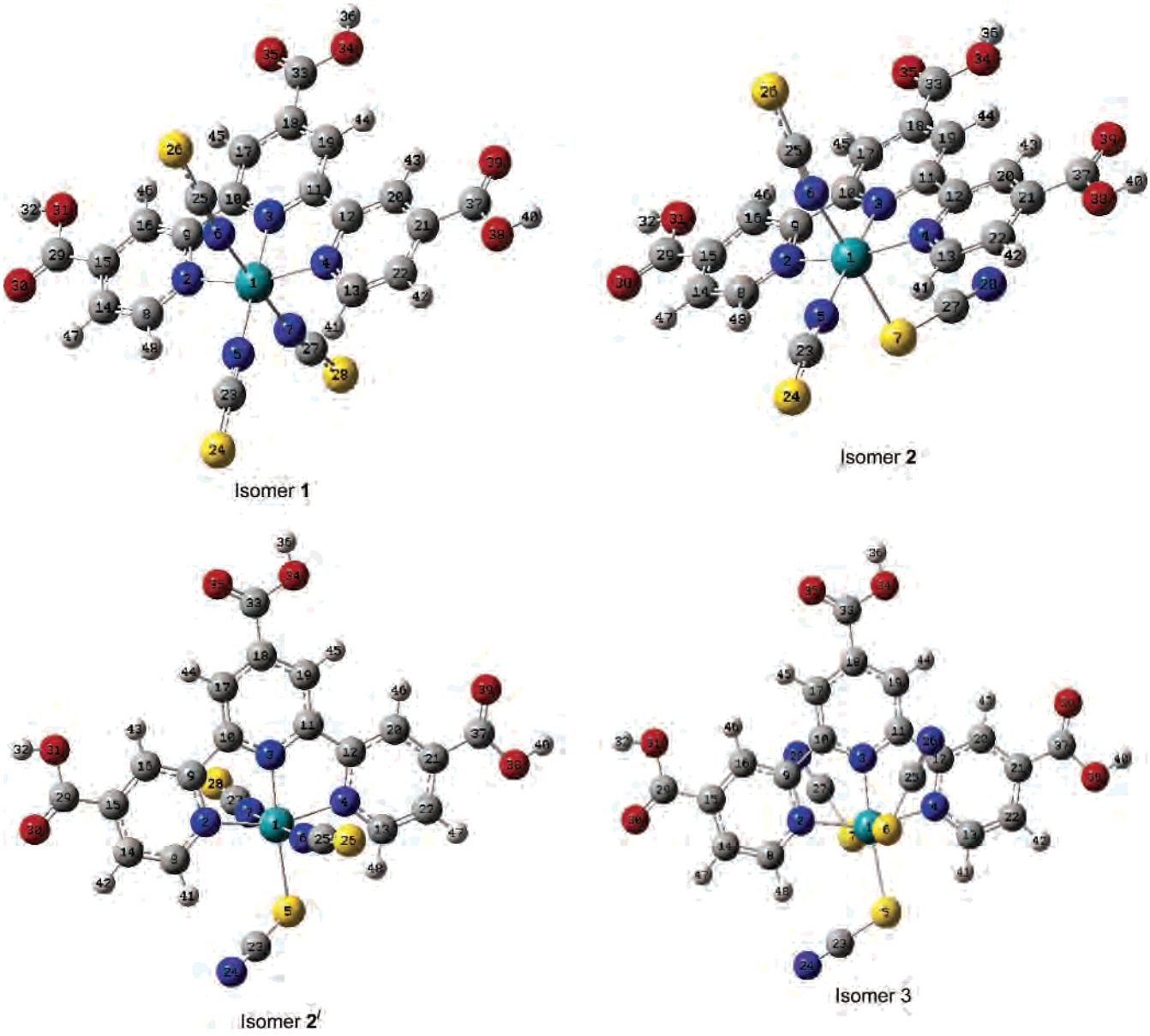

Figure 1. Optimized geometries of the four linkage isomers. (The atomic labels shown here are used in text).

of the distorted octahedral structure in these four isomers. In isomer **1**, one isothiocyanate occupies an equatorial position, and other two isothiocyanates occupy axial positions. In isomer **2**, two possibilities exist. Here, one thiocyanate can occupy one equatorial position or any one of the two axial positions. It is found that one thiocyanate in an axial position (isomer **2**) is more stable by approximately 4 kcal/mol than one with the thiocyanate in the equatorial position (isomer **2′**). Both isomers are considered in this study. In isomer **3**, one thiocyanate occupies an equatorial position, and the other two S-coordinated thiocyanates occupy axial positions. It has been found for BD, which has three isothiocyanate ligands coordinated to the metal through small nitrogen (−NCS), that the hybridizations of nitrogen to the metal and nitrogen to carbon have less p character than other isomers (with −SCN) which have a hybridization of the metal to sulfur bond and the sulfur to carbon bond. This could be the cause of the larger distortion which reduces the symmetry of isomers **2**, **2′**, and **3** compared to that of isomer **1**.

In all the four isomers, a donation from the σ orbital of the ligand toward an empty d orbital of the metal and a concurrent donation from a filled d orbital to a π^* antibonding orbital of the ligand is taking place, and the two processes promote and strengthen each other. Since polypyridine ligands have σ-donor orbitals localized on N and π-donor and π^*-acceptor orbitals delocalized[45] on aromatic rings, back-donation between the ligand and the Ru orbitals is significant. For isomer **1**, the calculated bond lengths and angles are found to be in good agreement with the experimental results. The Ru−N2 and Ru−N4 bond lengths of the pyridines opposite to each other are nearly the same. On the

(45) Boulet, P.; Chermette, H.; Daul, C.; Gilardoni, F.; Rogemond, F.; Weber, J.; Zuber, G. *J. Phys. Chem. A* **2001**, *105*, 885.

Table 1. Selected Geometrical Parameters for the Four Isomers Calculated under Different Levels of Theory (experimental values for isomer **1** are also shown)[a]

isomer **1**

geometry params[b]	G03w	ADF		
	mPW[c,d]	mPW[d,e]	mPW[d]	exptl[f]
Ru−N2	2.060	2.055	2.066	2.058(14)
Ru−N3	1.932	1.932	1.946	1.908(12)
Ru−N4	2.058	2.051	2.063	2.059(13)
Ru−N5	2.06	2.05	2.06	2.09(2)
Ru−N6	2.04	2.03	2.04	2.01(2)
Ru−N7	2.04	2.03	2.04	2.02(2)
∠N5RuN7	89.9	89.3	89.1	90.1(6)
∠N5RuN2	99.9	99.8	100.0	104.8(6)
∠N2RuN6	90.1	90.2	90.3	86.0(6)
∠N3RuN6	90.1	90.7	90.9	92.6(6)
∠N3RuN4	80.3	80.4	80.2	80.6(5)
∠N3RuN7	90.1	90.7	90.9	88.4(6)

isomer **2**[g]

geometry params[b]	G03w	ADF	
	mPW[c,d]	mPW[d,e]	mPW[d]
Ru−N2	2.050 [2.089]	2.044 [2.077]	2.058 [2.088]
Ru−N3	1.935 [1.942]	1.930 [1.951]	1.946 [1.962]
Ru−N4	2.063 [2.064]	2.055 [2.062]	2.075 [2.075]
Ru−N5 [Ru−S5]	2.07 [2.47]	2.06 [2.46]	2.07 [2.47]
Ru−N6	2.04 [2.03]	2.03 [2.01]	2.05 [2.03]
Ru−S7 [Ru−N7]	2.46 [2.04]	2.46 [2.02]	2.48 [2.04]
∠N5RuS7	84.7	83.2	83.3
[∠S5RuN7]	[87.3]	[86.8]	[86.8]
∠N5RuN2	99.0	98.3	98.6
[∠S5RuN2]	[105.2]	[105.1]	[105.3]
∠N2RuN6	90.3[89.8]	90.9[90.6]	90.8[90.6]
∠N3RuN6	88.9[92.2]	92.5[92.9]	92.5[92.9]
∠N3RuN4	80.1[80.1]	80.1[80.0]	79.7[79.8]
∠N3RuS7	94.6	95.2	95.2
[∠N3RuN7]	[88.7]	[89.6]	[89.6]

isomer **3**

geometry params[b]	G03w	ADF	
	mPW[c,d]	mPW[d,e]	mPW[d]
Ru−N2	2.083	2.070	2.092
Ru−N3	1.947	1.944	1.961
Ru−N4	2.062	2.049	2.072
Ru−S5	2.48	2.46	2.48
Ru−S6	2.47	2.48	2.49
Ru−S7	2.45	2.45	2.47
∠S5RuS7	87.3	84.5	84.6
∠S5RuN2	105.5	105.7	106.2
∠N2RuS6	91.4	91.6	91.8
∠N3RuS6	93.6	95.8	95.7
∠N3RuN4	79.9	80.0	79.7
∠N3RuS7	95.5	98.0	97.8

[a] Experimental geometry parameters are available for BD only (ref 42). [b] Bond lengths are in angstroms; bond angles are in degrees. [c] 6-31G(d,p) on H, N, S, C, O and LANL2DZ on Ru. [d] mPW refers to mPWx and PW91c together. [e] With SR-ZORA. [f] An asymmetric unit of this crystal structure contains two Ru(II) complexes with different bond lengths. We have tabulated the one closest to the optimized geometry; esd values are given in parentheses. [g] Values in square brackets indicate the geometry of isomer **2**.

other hand, the Ru−N3 bond length is smaller than Ru−N2 and Ru−N4. This is attributed to the steric effects of the thiocyanate/isothiocyanate ligand. It is found that the Ru−N2 distance is largest in isomer **3**, among all molecules, which is the result of the steric effect caused by the presence of thiocyanate ligand. Moreover, in isomers **1** and **2**, the π-back-donation from the central pyridine, which is trans to more electron-donating negatively charged isothiocyanate ligand, to the metal is less than that of the two peripheral pyridine rings, which are less electron-donating than the −NCS (or −SCN) ligand. Again, Ru−N6 and Ru−N7 have equal bond lengths which are smaller than Ru−N2, Ru−N4, and Ru−N5 in the case of isomer **1**. This is attributed to the lesser steric hindrance at the axial positions and more L → M back-bonding at the axial position of isomer **1**, and these are more electron-donating than the pyridine rings in the equatorial positions and trans to each other. But in case of isomers **2**, **2′**, and **3** having one and two axial thiocyanate ligands, respectively, which are coordinated to Ru through sulfur, the axial bond lengths (i.e., Ru−S7 for isomer **2** and Ru−S6 and Ru−S7 for isomer **3**) are larger than the Ru−N2, Ru−N3, and Ru−N4 bonds. The bond lengths in isomer **2′** are almost same as those in isomer **2.** We also find from the table that inclusion of the SR-ZORA improves the bond lengths, although there is not much of change in the bond angle.

To understand the nature of bonding interactions in the four isomers, we have carried out natural bond orbital (NBO)[46] analysis. To carry out this analysis, we first generate FILE 47 from the NBO subroutine of the ADF program using the TZ2P all-electron basis set and geometries obtained by ADF/mPW from Table 1, and then we use this as an input to the GENNBO routine.[46] The NBO theory provides the orthogonalized and linearized basis sets for the one-center (core and valence lone pairs), two-center (bonding and antibonding), three-center four-electron (if possible), and Rydberg-type molecular orbitals on the basis of the occupation of the electrons in that corresponding orbital. The additional advantage comes from this NBO approach as it mimics the localized Lewis-type molecular orbital pictures and corresponding localized bonds. Even the small residual energy values and charge contributions in the saturated systems are caused by the delocalization and noncovalent interactions. This noncovalence or hyperconjugated interactions are estimated by the NBO method as the second-order correction to interaction energy, $E(2)$, between the occupied molecular orbitals (donor, i) and the neighboring unoccupied molecular orbitals (acceptor, j).[47] This interaction energy represents the charge delocalization resulting from the loss of electronic occupation from the localized Lewis molecular orbital to the non-Lewis molecular orbital leading to the distribution of electronic charge and thus the perturbation from idealized Lewis structure description. The interaction energy (stabilization energy), $E(2)$, associated with the delocalization occurred (2e stabilization) between the donor NBO (i) and the acceptor NBO (j) can be estimated from eq 2.

$$E(2) = \Delta E_{ij} = q_i/[F(i,j)^2(e_j - e_i)] \qquad (2)$$

where q_i is the donor orbital occupancy, e_i and e_j are the

(46) Glendening, E. D.; Badenhoop, J. K.; Reed, A. E.; Carpenter, J. E.; Bohmann, J. A.; Morales, C. M.; Weinhold, F. *NBO 5.0*; Theoretical Chemistry Institute, University of Wisconsin: Madison, WI, 2001; http://www.chem.wisc.edu/~nbo5.

diagonal elements (orbital energies), and $F(i, j)$ is the off-diagonal NBO Fock matrix element.

From second-order perturbation energy analysis and after the analysis of all the possible orbital interactions, the main charge delocalization can be broadly classified into two groups. They are (1) the donation of electronic charge from the metal to ligand and (2) the back-donation of electronic charge from ligand to metal. The interaction energies, $E(2)$, larger than 25.0 kcal/mol are listed in Table 2, along with the calculated natural charges. The interactions from metal to ligand are very small and, hence, are not tabulated. Because the back-donation exists in the four isomers and also the negative charge of −1 is expected to be stabilized on the ligands, the next thing is to study the extent of back-donation to understand the spectrum and help us to explain the observed blue shift with the S-bonded isomers (isomer **2** and isomer **3**) compared to the N-bonded isomer (isomer **1**). In isomer **1**, there is more back-donation from the peripheral pyridine rings and equatorial isothiocyanate ligands than from the central ring and axial isothiocyanate ligands, respectively. Here, the lone pair on nitrogen of the one of the side pyridine rings with an occupancy of 1.655e has an interaction with the $d_{x^2-y^2}$ and s orbitals of Ru with occupancies of 0.872e and 0.163e by 429.3 and 209.3 kcal/mol of interaction energy, respectively. The lone pair from another peripheral pyridine ring interact with the same $d_{x^2-y^2}$ and s orbitals of Ru which results in stabilization by 440.2 kcal/mol and 209.3 kcal/mol, respectively. The lone pair of the central pyridine nitrogen with an occupancy of 1.588e has charge delocalization resulting from the s orbital of Ru, which gives a delocalization energy of 234.5 kcal/mol. In a similar way, the lone pair from the equatorial −NCS nitrogen with an occupancy of 1.695e has an interaction with the above-mentioned Ru lone pairs along with another d_{z^2} orbital with 0.922e occupation by 662.6, 250.5, and 263.1 kcal/mol, respectively. Similarly the $sp^{1.10}$ orbital from the axial −NCS nitrogen with an occupancy of 1.650e interacts with the above-mentioned orbitals of Ru by 435.5, 115.3, and 235.0 kcal/mol, respectively. Because of the symmetry, the lone pair from another axial −NCS nitrogen also contributes same energy values.

In isomer **2**, a major back-donation also takes place through the peripheral pyridine rings, but here, the amount of stabilization energy resulting through these interactions varies according to the ligand. Here, the delocalizations resulting from the interactions, such as $n-\sigma^*$, show the charge dispersion nature in this isomer. In isomer **3**, the electrostatic interactions from both the aromatic terpyridine and anionic thiocyanate ligands are reduced compared to the above two isomers, and because of this, the charge dispersive interactions are more in isomer **3** than in isomers **1** and **2**. Finally, it is clear from the table that the interaction between Ru and both the aromatic and anionic ligands is less in isomer **2′** than in isomer **1**.

(47) (a) Reed, A. E.; Weinstock, R. B.; Weinhold, F. *J. Chem. Phys.* **1985**, *83*, 735. (b) Reed, A. E.; Weinhold, F.; Curtiss, L. A. *Chem. Rev.* **1988**, *88*, 899.

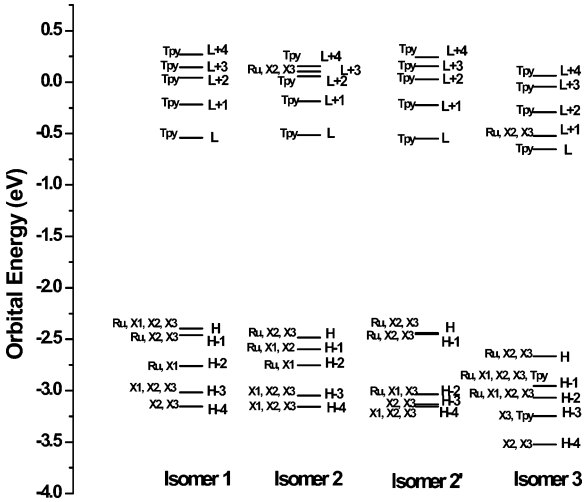

Figure 2. Pictorial representation of the molecular orbital energy levels (five highest-occupied and five lowest-unoccupied) of the four linkage isomers calculated in ethanol at the LB94/TZP level. In isomer **1**, the labels denote that X1 = equatorial −NCS, X2 and X3 = axial −NCS; in isomer **2**, X1 = equatorial −NCS, X2 = axial −NCS, X3 = axial −SCN; in isomer **2′**, X1 = equatorial −SCN, X2 and X3= axial −NCS; and in isomer **3**, X1 = equatorial −SCN, X2 and X3 = axial −SCN. Tpy corresponds to the terpyridene rings. Here, H refers to the HOMO and L to the LUMO.

From the last column of the same table, one can see the natural charges obtained from the NBO analysis. The Ru metal has a positive charge of 0.949 and the tpy ligand is −0.080 in isomer **1**. The three NCS units together have the charge of −1.869. Thus, the negative charge is stabilized on the NCS moieties. There is a small change of the charge on the Ru in isomer **2** (**2′**), and but there is also a decrease of the negative charge on the 2 NCS and 1 SCN moieties. Here, the charges are 0.854 (0.856) and −1.802 (−1.763), respectively. In isomer **3**, there is still a further decrease in the charge on Ru, which his now only 0.606, and for the SCN moieties, a value of only −1.540 is seen.

(b) Electronic Structure (in solvent). The ground-state electronic structure is calculated to determine the energies and compositions of the MOs. From the literature, it is evident that the calculations on Ru dyes performed in gas phase cannot be compared with the experimental results of the electronic structure and UV spectra, and for this reason, solvent effects should be incorporated into the calculations.[39] To understand the electronic structure and absorption spectra, the solvent effect (ethanol) is included in these calculations. The frontier orbitals obtained using the COSMO option are plotted according to their energies in Figure 2. The assignment of the type of each MO was made on the basis of its composition (Table 3) and by visual inspection of its three-dimensional representation. The three highest-occupied MOs (HOMO, HOMO−1, and HOMO−2) of three complexes consists of Ru d orbitals and are antibonding with respect to the isothiocyanate ligands as shown by the appreciable electron density on the nitrogen, carbon, and sulfur atoms. Because of the introduction of the strong donor isothiocyanate ligand, the metal HOMO level is destabilized, and the energy gap between highest-occupied molecular orbitals (HOMO) and lowest-unoccupied molecular orbitals (LUMOs) (i.e., HOMO − LUMO) is decreased. The energy of

Table 2. Second-Order Perturbation Interaction Energy ($E(2)$) from the Donation from Ligand to Metal and NPA Charges on Ru, Terpyridine (Tpy), and Three Thiocyanate/Isothiocyanate ($[NCS]_3$) Groups in All the Four Isomers at the mPWx, PW91C/TZ2P Level Obtained by NBO Analysis[a]

isomer **1**

donor	occupancy (e)	acceptor[b]	occupancy (e)	$E(2)$ (kcal/mol)	charges from natural orbitals
$(sp^{2.37})_{N2}$	1.655	$(d_{x^2-y^2})_{Ru}$	0.872	429.3	Ru (0.949)
$(sp^{2.37})_{N2}$	1.655	$(s)_{Ru}$	0.163	209.3	Tpy (−0.080)
$(sp^{2.62})_{N3}$	1.588	$(s)_{Ru}$	0.163	234.5	$[NCS]_3$ (−1.869)
$(sp^{2.37})_{N4}$	1.652	$(d_{x^2-y^2})_{Ru}$	0.872	440.2	
$(sp^{2.37})_{N4}$	1.652	$(s)_{Ru}$	0.163	209.3	
$(sp^{1.09})_{N5}$	1.695	$(d_{z^2})_{Ru}$	0.922	662.6	
$(sp^{1.09})_{N5}$	1.695	$(d_{x^2-y^2})_{Ru}$	0.872	250.5	
$(sp^{1.09})_{N5}$	1.695	$(s)_{Ru}$	0.163	263.1	
$(sp^{1.10})_{N6}$	1.650	$(d_{z^2})_{Ru}$	0.922	435.5	
$(sp^{1.10})_{N6}$	1.650	$(d_{x^2-y^2})_{Ru}$	0.872	115.3	
$(sp^{1.10})_{N6}$	1.650	$(s)_{Ru}$	0.163	235.0	
$(sp^{1.10})_{N7}$	1.650	$(d_{z^2})_{Ru}$	0.922	435.4	
$(sp^{1.10})_{N7}$	1.650	$(d_{x^2-y^2})_{Ru}$	0.872	115.3	
$(sp^{1.10})_{N7}$	1.650	$(s)_{Ru}$	0.163	234.9	

isomer **2**

donor	occupancy (e)	acceptor[b]	occupancy (e)	$E(2)$ (kcal/mol)	charges from natural orbitals
$(sp^{2.39})_{N2}$	1.657	$(d_{x^2-y^2})_{Ru}$	0.869	317.6	Ru (0.854)
$(sp^{2.39})_{N2}$	1.657	$(s)_{Ru}$	0.199	225.2	Tpy (−0.053)
$(sp^{2.39})_{N2}$	1.657	$0.823\ (sd^{17.37})_{Ru} - 0.568\ (sp^{11.23})_{S7}$	0.529	93.3	$[NCS]_3$ (−1.802)
$(sp^{2.64})_{N3}$	1.599	$(s)_{Ru}$	0.199	252.9	
$(sp^{2.64})_{N3}$	1.599	$0.823\ (sd^{17.37})_{Ru} - 0.568\ (sp^{11.23})_{S7}$	0.529	102.2	
$(sp^{2.43})_{N4}$	1.662	$(d_{x^2-y^2})_{Ru}$	0.869	330.3	
$(sp^{2.43})_{N4}$	1.662	$(s)_{Ru}$	0.199	226.5	
$(sp^{2.43})_{N4}$	1.662	$0.823\ (sd^{17.37})_{Ru} - 0.568\ (sp^{11.23})_{S7}$	0.529	92.6	
$(sp^{1.10})_{N5}$	1.698	$(d_{x^2-y^2})_{Ru}$	0.869	498.2	
$(sp^{1.10})_{N5}$	1.698	$(s)_{Ru}$	0.199	281.9	
$(sp^{1.10})_{N5}$	1.698	$0.823\ (sd^{17.37})_{Ru} - 0.568\ (sp^{11.23})_{S7}$	0.529	112.3	
$(sp^{1.06})_{N6}$	1.652	$(s)_{Ru}$	0.199	202.4	
$(sp^{1.06})_{N6}$	1.652	$0.823\ (sd^{17.37})_{Ru} - 0.568(sp^{11.23})_{S7}$	0.529	298.2	

isomer **2′**

donor	occupancy (e)	acceptor[b]	occupancy (e)	$E(2)$ (kcal/mol)	charges from natural orbitals
$(sp^{2.34})_{N2}$	1.664	$(d_{x^2-y^2})_{Ru}$	0.872	307.8	Ru (0.856)
$(sp^{2.34})_{N2}$	1.664	$(s)_{Ru}$	0.174	206.5	Tpy (−0.093)
$(sp^{2.55})_{N3}$	1.596	$(d_{z^2})_{Ru}$	0.980	795.6	$[NCS]_3$ (−1.763)
$(sp^{2.55})_{N3}$	1.596	$(d_{x^2-y^2})_{Ru}$	0.872	170.2	
$(sp^{2.55})_{N3}$	1.596	$(s)_{Ru}$	0.174	193.7	
$(sp^{2.35})_{N4}$	1.656	$(d_{x^2-y^2})_{Ru}$	0.872	268.6	
$(sp^{2.35})_{N4}$	1.656	$(s)_{Ru}$	0.174	200.5	
$(sp^{9.28})_{S5}$	1.528	$(s)_{Ru}$	0.174	236.6	
$(sp^{1.12})_{N6}$	1.649	$(d_{z^2})_{Ru}$	0.980	210.1	
$(sp^{1.12})_{N6}$	1.649	$(d_{x^2-y^2})_{Ru}$	0.872	373.7	
$(sp^{1.12})_{N6}$	1.649	$(s)_{Ru}$	0.174	252.5	
$(sp^{1.11})_{N7}$	1.654	$(d_{z^2})_{Ru}$	0.980	182.7	
$(sp^{1.11})_{N7}$	1.654	$(d_{x^2-y^2})_{Ru}$	0.872	325.8	
$(sp^{1.11})_{N7}$	1.654	$(s)_{Ru}$	0.174	245.9	

isomer **3**

donor	occupancy (e)	acceptor[b]	occupancy (e)	$E(2)$ (kcal/mol)	charges from natural orbitals
$(sp^{2.40})_{N2}$	1.675	$(d_{x^2-y^2})_{Ru}$	0.896	43.5	Ru (0.606)
$(sp^{2.40})_{N2}$	1.675	$(s)_{Ru}$	0.224	238.8	Tpy (−0.066)
$(sp^{2.40})_{N2}$	1.675	$0.793\ (sd^{16.44})_{Ru} - 0.609(sp^{11.72})_{S7}$	0.620	107.6	$[NCS]_3$ (−1.540)
$(sp^{2.62})_{N3}$	1.612	$(d_{x^2-y^2})_{Ru}$	0.896	493.1	
$(sp^{2.62})_{N3}$	1.612	$(s)_{Ru}$	0.224	224.5	
$(sp^{2.62})_{N3}$	1.612	$0.793\ (sd^{16.44})_{Ru} - 0.609\ (sp^{11.72})_{S7}$	0.620	101.4	
$(sp^{2.41})_{N4}$	1.666	$(d_{x^2-y^2})_{Ru}$	0.896	50.3	
$(sp^{2.41})_{N4}$	1.666	$(s)_{Ru}$	0.224	234.0	
$(sp^{2.41})_{N4}$	1.666	$0.793\ (sd^{16.44})_{Ru} - 0.609\ (sp^{11.72})_{S7}$	0.620	104.8	
$(sp^{8.18})_{S5}$	1.542	$(s)_{Ru}$	0.224	301.2	
$(sp^{8.18})_{S5}$	1.542	$0.793\ (sd^{16.44})_{Ru} - 0.609\ (sp^{11.72})_{S7}$	0.620	252.6	
$(sp^{15.01})_{S6}$	1.434	$(s)_{Ru}$	0.224	250.3	
$(sp^{15.01})_{S6}$	1.434	$0.793\ (sd^{16.44})_{Ru} - 0.609\ (sp^{11.72})_{S7}$	0.620	473.4	

[a] Value of $E(2)$ is calculated from eq 1. [b] Only the dominant character is indicated.

Table 3. Kohn−Sham Orbitals with Dominant Character (%) and the Energy (eV) of the Orbitals for the Four Linkage Isomers Calculated in Ethanol at the LB94/TZP Level[a]

isomer **1**

		dominant character (%)		
orbital	energy (eV)	Ru[b]	[NCS]	Tpy
LUMO+4 (71A′)	0.269			7 (L3), 8 (C1), 84 (C3)
LUMO+3 (32A″)	0.144			28 (L1), 32 (L2), 19 (L3), 6 (C1), 10 (C2), 4(C3)
LUMO+2 (31A″)	0.043			35 (L1), 7 (L2), 41 (L3), 7 (C1), 9(C3)
LUMO+1 (30A″)	−0.217			28 (L1), 40 (L2), 25 (L3), 3 (C1), 3 (C3)
LUMO (29A″)	−0.542			24 (L1), 30 (L2), 27 (L3), 5 (C1) 5 (C2), 5 (C3)
HOMO (28A″)	−2.396	30 (d_{yz})	14 (X1), 50 (X2, X3)	5 (L2)
HOMO−1 (27A″)	−2.460	29 (d_{xz})	71 (X2, X3)	
HOMO−2 (70A′)	−2.762	31 (d_{xy})	67 (X1)	
HOMO−3 (26A″)	−3.016		67 (X1), 33 (X2, X3)	
HOMO−4 (69A′)	−3.153	2 (p_x)	3 (X1), 95 (X2, X3)	

isomer **2**

		dominant character (%)		
orbital	energy (eV)	Ru[b]	[NCS]	Tpy
LUMO+4 (103A)	0.155			20(L1), 33(L2), 26(L3), 4 (C1), 12 (C2), 5 (C3)
LUMO+3 (102A)	0.102	54 (d_{z^2})	10 (X2), 23 (X3)	3 (L1), 4 (L3)
LUMO+2 (101A)	0.056			41 (L1), 8 (L2), 35 (L3), 8(C1), 7 (C3)
LUMO+1 (100A)	−0.187			25 (L1), 40 (L2), 27 (L3), 3 (C1), 4 (C3)
LUMO (99A)	−0.516			28(L1), 27(L2), 25(L3), 5 (C1), 5 (C2), 5 (C3)
HOMO (98A)	−2.483	31 (d_{xz})	4(X1), 36 (X2), 24 (X3)	4 (L2)
HOMO−1 (97A)	−2.597	30 (d_{yz})	23 (X1), 39 (X2), 2 X(3)	6 (L2)
HOMO−2 (96A)	−2.752	35 (d_{xy})	63 (X1)	
HOMO−3 (95A)	−3.048		45 (X1), 39 (X2), 16 (X3)	
HOMO−4 (94A)	−3.156		10 (X1), 53 (X2), 36 (X3)	

isomer **2′**

		dominant character (%)		
orbital	energy (eV)	Ru[b]	[NCS]	Tpy
LUMO+4 (103A)	0.243			9 (L3), 3 (C1), 84 (C3)
LUMO+3 (102A)	0.154			39 (L1), 30 (L2), 10 (L3), 8 (C1), 10 (C2)
LUMO+2 (101A)	0.028			23 (L1), 6 (L2), 54 (L3), 5 (C1), 11 (C3)
LUMO+1 (100A)	−0.224			29 (L1), 37 (L2), 25 (L3), 3 (C1), 4 (C3)
LUMO (99A)	−0.549	4 (d_{yz})		23 (L1), 31 (L2), 28 (L3), 4 (C1), 5 (C2), 5 (C3)
HOMO (98A)	−2.439	29 (d_{xz}, d_{yz})	38 (X2), 31 (X3)	
HOMO−1 (97A)	−2.451	29 (d_{xz}, d_{yz})	37 (X2), 34 (X3)	
HOMO−2 (96A)	−3.036	13 (d_{xy})	64 (X1), 2 (X2), 21 (X3)	
HOMO−3 (95A)	−3.133	2 (d_{xy})	2 (X1), 44 (X2), 52 (X3)	
HOMO−4 (94A)	−3.153		13 (X1), 55 (X2), 31 (X3)	

isomer **3**

		dominant character (%)		
orbital	energy (eV)	Ru[b]	[NCS]	Tpy
LUMO+4 (103A)	0.062			40 (L1), 29 (L2), 14 (L3), 7 (C1), 10 (C2)
LUMO+3 (102A)	−0.044			27 (L1), 6 (L2), 52 (L3), 5 (C1), 9 (C3)
LUMO+2 (101A)	−0.293			28 (L1), 37 (L2), 27 (L3), 3 (C1), 3 (C3)
LUMO+1 (100A)	−0.523	48 (d_{z^2})	3 (X1), 20 (X2), 24 (X3)	
LUMO (99A)	−0.652			23 (L1), 29 (L2), 29 (L3), 4 (C1), 5 (C2), 5 (C3)
HOMO (98A)	−2.664	34 (d_{xz})	22 (X2), 32 (X3)	3 (L1), 4 (L2), 4(L3)
HOMO-1 (97A)	−2.956	39 (d_{yz})	10 (X1), 17 (X2), 15 (X3)	16 (L2)
HOMO-2 (96A)	−3.068	30 (d_{xy})	35 (X1), 22 (X2), 11 (X3)	
HOMO-3 (95A)	−3.246	2 (d_{yz})	5 (X2), 9 (X3)	22 (L1), 47 (L2), 15 (L3)
HOMO-4 (94A)	−3.524	2 (p_z)	4 (X1), 43 (X2), 46 (X3)	

[a] In isomer **1**, X1 = equatorial −NCS, X2 and X3= axial −NCS; in isomer **2**, X1= equatorial −NCS, X2= axial −NCS, X3= axial −SCN; in isomer **2′**, X1 = equatorial −SCN, X2 and X3= axial −NCS; in isomer **3**, X1= equatorial −SCN, X2 and X3= axial −SCN; L1, L2, L3 are tpy ligands, while C1, C2, C3 are the carboxylic acid groups. [b] For Ru, dominant orbital character is given in parentheses.

HOMO and LUMO levels shows that the introduction of three electron-donating −NCS ligands results in a larger destabilization on the HOMO orbital of isomer **1** than the introduction of two −NCS ligands and one −SCN ligand in isomer **2** or **2′**, which again has a larger destabilization of the HOMO level than isomer **3** with three −SCN ligands. On the other hand, stabilization of the LUMO levels is more prominent in the latter three cases, and the order of stabilization of LUMO levels is as follows: **3** > **2′** > **1** > **2**. This means that the order of the energy gap between HOMO and LUMO decreases with the addition of a good electron-donating group. The HOMO − LUMO gaps of isomers **1**, **2**, **2′**, and **3** are 1.85, 1.97, 1.89, and 2.01 eV, respectively. Here, the role of the isothiocyanate ligands is

to tune the metal t_{2g} orbitals of Ru(II) and possibly to stabilize the hole that is being generated on the metal, after an electron was injected into the conduction band. The next important orbitals involved in the transitions are the HOMO−1 and HOMO−2. The energy differences between the HOMO and HOMO−1 levels are 0.06, 0. 11, 0.01, and 0.29 eV for isomers **1**, **2**, **2′**, and **3**, respectively, and the energy differences between the HOMO and HOMO−2 are 0.37, 0.27, 0.60, and 0.40 eV for isomers **1**, **2**, **2′**, and **3**, respectively. This indicates that the energy gap between HOMO and HOMO−1 of isomer **3** is more than that of isomers **1**, **2**, and **2′**.

It will be useful to examine the character of the highest-occupied and lowest-virtual orbitals for these Ru complexes to provide the framework for the excited-state TD-DFT calculations in the subsequent section. The assignment of the type of each MO is made on the basis of its composition shown in Table 3, in which only the most important five occupied and five virtual (unoccupied) orbitals are listed, together with orbital compositions expressed in terms of the compositions from the Ru central atom, axial and equatorial −NCS or −SCN ligands, and tpy ligand.

In isomer **1**, the HOMO (28A″) consists of 94% Ru and −NCS character [30% Ru d + (14% X1 + 50% X2 and X3) 64% −NCS], while the LUMO (29A″) consists of 96% terpyridine and COOH character (81% terpyridine + 15% COOH). In isomer **2**, the HOMO (98A) is 95% Ru, −NCS, and −SCN character (31% Ru d + 24% −SCN + 40% −NCS), while the LUMO (99A) is 95% terpyridine and COOH character (80% terpyridine + 15% COOH). In isomer **2′**, the HOMO (98A) is 98% Ru and −NCS character (29% Ru d + 69% −NCS), while the LUMO (99A) is 96% terpyridine and COOH character (82% terpyridine + 14% COOH). In isomer **3**, the HOMO (98A) consists of 88% metal and −SCN character (34% metal + 54% −SCN), and the LUMO (99A) consists of 95% metal and terpyridine character (81% terpyridine + 14% COOH). In the HOMO, HOMO−1, and HOMO−2, the electron density is strongly delocalized over metal Ru and the thiocyanate ligand in isomer **1**. In HOMO−3 and HOMO−4, the metal contributions are negligible. The five lowest LUMOs for isomer **1** are calculated to be almost exclusively located on the terpyridine ligand.

Similarly, in isomers **2′**, **2**, and **3**, the highest-occupied molecular orbitals have more metal and isothiocyanate or thiocyanate contributions, except for the HOMO−3 of isomer **3** (which has 84% terpyridine contribution, 2% metal contribution, and 14% thiocyanate contribution). The LUMO and the other virtual orbitals have more terpyridine contributions, except for the LUMO+1 of isomer **3** (which has 47% thiocyanate contribution and 48% Ru contribution) and the LUMO+3 of isomer **2** (which has 54% Ru contribution, 23% thiocyanate contribution, and 10% isothiocyanate contribution). Thus, the HOMOs in all four isomers have significant d-metal character, but contributions also come from the −NCS or −SCN ligands, while the LUMOs are mainly localized on terpyridine ligand and little contribution is there from d orbitals of metal atoms. Orbitals obtained in the gas phase calculations, differ significantly from orbitals obtained using solvent both in composition and energy levels, as expected. [39a]

A comparison between the orbital energies of the isomers of the BD complex in the gas phase and in ethanol can easily explain the solvent effect of ethanol on the isomers. Inclusion of solvent effects shows a significant change of both energies and composition of the molecular orbitals. In ethanol, both the HOMO and LUMO of isomer **1** are significantly destabilized by 4.862 and 6.359 eV, respectively, compared to isomer **1** in the gas phase. This calculation also shows a lower contribution of the Ru d orbitals mixed with NCS ligand orbitals in ethanol solvent (i.e., 94% compared to the contributions in the gas phase which is 98%). For isomer **2** in ethanol, the HOMO is destabilized by 4.777 eV, and LUMO is destabilized by 6.408 eV. For isomer **2′**, the HOMO is destabilized by 4.858 eV, and LUMO is destabilized by 6.412 eV. Here, for isomer **2**, the contribution of Ru d orbitals mixed with NCS ligand orbitals in gas phase is 98.8%, while in ethanol solvent, this contribution is 95%. For isomer **2′**, the contribution of Ru d orbitals mixed with the NCS ligand orbitals in the gas phase is 90.0%, and in ethanol solvent, this contribution is 98%. For isomer **3**, the HOMO is destabilized by 4.823 eV, and LUMO is destabilized by 6.343 eV. Here, for isomer **3**, the contribution of Ru d orbitals mixed with NCS ligand orbitals in gas phase is 83.2%, while in ethanol solvent, this contribution is 88%. Thiocyanate, isothiocyanate, and metal contributions to the HOMOs which are involved as a starting level in the observed absorption bands and the contribution of terpyridine with carboxylate in LUMOs have an important role for the electron injection and regeneration of the dye-sensitized TiO_2 solar cells. From the above results, it can be predicted that the LUMO level for each isomer is more destabilized than the HOMO level. Altogether, in ethanol solvent, the HOMO−LUMO gap increases significantly for each isomer of BD. The results of the BD isomers can be compared with the results of the N3 dye in ethanol solvent where the HOMO level in ethanol solvent is stabilized and the LUMO level is destabilized but HOMO−LUMO gap is increased like all isomers of BD.[37e] For isomer **1** of BD, in ethanol, the HOMO−LUMO gap is −1.854 eV, whereas in the gas phase, the HOMO−LUMO gap is −0.357 eV. For isomer **2**, in ethanol, the HOMO−LUMO gap is −1.967 eV, whereas in the gas phase, the HOMO−LUMO gap is −0.336 eV. For isomer **2′**, in ethanol, the HOMO−LUMO gap is −1.890 eV, whereas in the gas phase, the HOMO−LUMO gap is −0.336 eV. For isomer **3**, in ethanol, the HOMO−LUMO gap is −2.012 eV, whereas in gas phase**,** the HOMO−LUMO gap is −0.492 eV. Thus, for all the isomers in BD, the HOMO−LUMO gap is increased in ethanol compared to the results in the gas phase.

(c) Optical Absorption Spectra (in solvent). The calculated electronic spectrum of the four isomers of BD in ethanol solvent by TDDFT calculations are given in Table 4−6, and the calculated electronic spectra of the four isomers of the BD in gas phase are given in the Supporting Information. The TDDFT results of all four isomers of BD in ethanol are

Table 4. Selected Lowest-Excitation Energies (ΔE), Oscillator Strengths (f), and Dominant Excitation Character for the Low-Lying Singlet State of Isomer **1** Calculated in Ethanol (LB94/ TZP)[a]

state	main configuration	ΔE (eV)	f	excitation character
1	0.749 (28a″ → 29a″) 0.224 (27a″→29a″)	1.94 (2.00)[b]	0.015	LLCT + MLCT LLCT + MLCT
2	0.768 (27a″ → 29a″) 0.217 (28a″ → 29a″)	1.95	0.014	LLCT + MLCT LLCT + MLCT
3	0.983 (28a″ → 30a″)	2.21	0.013	LLCT + MLCT
10	0.679 (28a″ → 32a″) 0.144 (27a″ → 31a″)	2.61	0.039	LLCT + MLCT LLCT + MLCT
12	0.911 (27a″ → 32a″)	2.63	0.016	LLCT + MLCT
20	0.586 (25a″ → 29a″) 0.331 (26a″ → 30a″)	2.84	0.040	LLCT LLCT

[a] Only f values greater than 0.010 are reported. [b] Experimental ΔE.[11,15]

Table 5. Selected Lowest-Excitation Energies (ΔE), Oscillator Strengths (f), and Dominant Excitation Character for the Low-Lying Singlet States of Isomers **2** and **2′** Calculated in Ethanol (LB94/ TZP)[a]

2

state	main configuration	ΔE (eV)	f	excitation character
1	0.920 (98a → 99a)	2.03 (2.10)[b]	0.014	LLCT + MLCT
2	0.901 (97a → 99a)	2.17	0.021	LLCT + MLCT
4	0.945 (98a → 100a)	2.35	0.012	LLCT + MLCT
6	0.966 (95a → 99a)	2.56	0.012	LLCT
10	0.646 (98a → 103a) 0.194 (97a → 101a)	2.68	0.013	LLCT + MLCT LLCT + MLCT
14	0.386 (97a → 103a) 0.238 (97a → 102a) 0.225 (93a → 99a)	2.79	0.019	LLCT + MLCT LLCT + MLCT LLCT
15	0.445 (97a → 102a) 0.169 (96a → 101a) 0.144 (93a → 99a)	2.79	0.012	LLCT + MLCT LLCT + MLCT LLCT
17	0.412 (93a → 99a) 0.396 (97a → 103a)	2.82	0.037	LLCT LLCT + MLCT

2′

state	main configuration	ΔE (eV)	f	excitation character
1	0.531 (97a → 99a) 0.463 (98a → 99a)	1.93 (2.10)[b]	0.013	LLCT + MLCT LLCT + MLCT
10	0.586 (97a → 102a) 0.354 (98a → 102a)	2.62	0.013	LLCT + MLCT LLCT + MLCT
11	0.449 (98a → 102a) 0.349 (97a → 102a)	2.65	0.020	LLCT + MLCT LLCT + MLCT
18	0.487 (93a → 99a) 0.433 (96a → 100a)	2.80	0.013	LLCT + MLCT LLCT + MLCT
19	0.535 (96a → 100a) 0.372 (93a → 99a)	2.85	0.034	LLCT + MLCT LLCT

[a] Only f values greater than 0.010 are reported. [b] Experimental ΔE.[11,15]

in good agreement with the experimental results. The UV−vis spectra of the four isomers of BD are dominated by MLCT and LLCT in the visible region. The λ_{max} value of the low-energy MLCT + LLCT band of isomer **1** is red shifted compared to those of the isomers **2** and **2′**, which are again red shifted compared to that of isomer **3**, as can be seen in Figure 3, generated by ADF spectra software using Gaussian broadening.[29] The red shift of the longer wavelength band on going from the fully S-bonded isomer to the fully N-bonded isomer is attributed to the stronger electron-donating power of the N-bonded isocyanate groups compared to the S-bonded thiocyanate, which increases the energy of metal d π orbitals. The character for each excited state is assigned using Figure 4. In the LLCT[48] excited state of the four isomers, the excited electron is localized on the terpyridine ligand, and the hole is localized on the isothiocyanate or thiocyanate ligands. On the other hand, in the MLCT excited states, the excited electron is localized on the terpyridine ligand, and the hole is localized on the Ru metal.

Table 6. Selected Lowest-Excitation Energies (ΔE), Oscillator Strengths (f), and Dominant Excitation Character for the Low-Lying Singlet State of Isomer **3** Calculated in Ethanol (LB94/ TZP)[a]

state	main configuration	ΔE (eV)	f	excitation character
1	0.991 (98a → 99a)	2.06 (2.18)[b]	0.010	LLCT + MLCT
5	0.385 (96a → 99a) 0.307 (97a → 99a) 0.175 (98a → 101a)	2.52	0.214	LLCT + MLCT LLCT + MLCT LLCT + MLCT
13	0.299 (95a → 99a) 0.212 (98a → 103a) 0.163 (97a → 101a) 0.144 (96a → 101a)	2.86	0.065	LLCT LLCT + MLCT LLCT + MLCT LLCT + MLCT
20	0.547 (97a → 103a) 0.200 (96a → 103a)	3.09	0.011	LLCT + MLCT LLCT + MLCT

[a] Only f values greater than 0.010 are reported. [b] Experimental ΔE.[11,15]

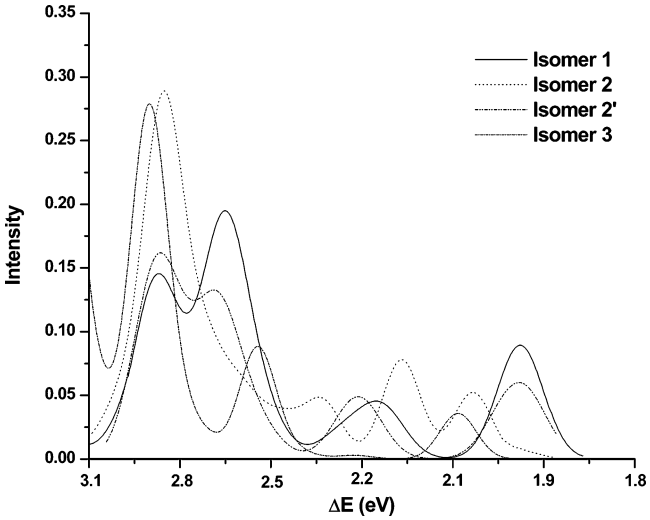

Figure 3. Absorption spectra for the four isomers computed in ethanol at the LB94/TZP level.

The experimental values of λ_{max} in ethanol solvents of isomers **1**, **2 (2′)**, and **3** correspond to energy values of 2.00, 2.10, and 2.18 eV, respectively, and the calculated theoretical λ_{max} values (using the ADF package) of isomers **1**, **2**, **2′**, and **3** in ethanol correspond to 1.94, 2.03, 1.93, and 2.06 eV, respectively. The value of 2.03 eV obtained for isomer **2** is in good agreement with the experimental value of 2.10 eV. Thus, the experimentally observed transitions could be attributed to isomer **2** and not **2′**, as observed from calculations.

In the time-dependent calculations, we are considering singlet → singlet spin allowed transitions. The λ_{max} transitions

(48) Crosby, G. A.; Highland, R. G.; Truesdell, K. A. *Coord. Chem. Rev.* **1985**, *64*, 41.

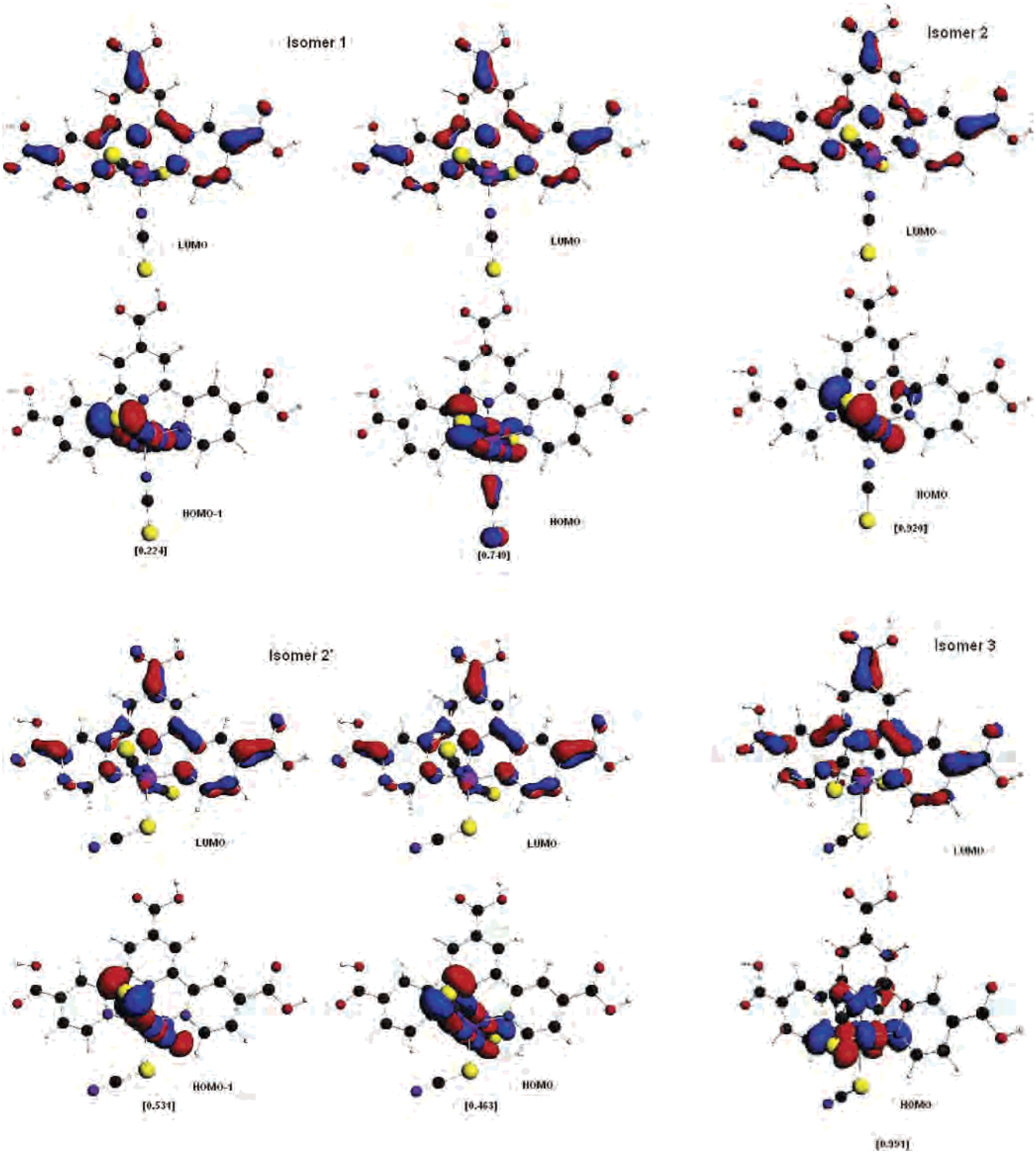

Figure 4. Frontier molecular orbital pictures of major contributors of four isomers obtained in ethanol at the LB94/TZP level (coefficients are given in parentheses).

of the four isomers with the contributions from the orbitals and oscillator strengths mentioned in parentheses are as follows: in isomer **1** ($f = 0.015$), HOMO → LUMO (0.749), HOMO−1 → LUMO (0.224); in isomer **2** ($f = 0.014$), HOMO → LUMO (0.920); in isomer **2′** ($f = 0.013$), HOMO−1 → LUMO (0.531), HOMO → LUMO (0.463)); and in isomer **3** ($f = 0.010$), HOMO → LUMO (0.991). It is expected that the excited states with significant oscillator strengths throughout the MOs, which are likely to be involved in bonding to the semiconductor, are those localized on the anchoring carboxylate moieties of the terpyridine ligands.[49] It is observed that there is significant electron localization on the carboxyl of central pyridine for LUMO level of isomer **1**. Thus in the isomer **1** configurations with

(49) Monat, J. E.; Rodriguez, J. H.; McCusker, J. K. *J. Phys. Chem. A.* **2002**, *106*, 7399.

97% contribution (from the excitation coefficient), there is significant electron localization on the carboxyl of central pyridine. In isomer **2**, there is significant electron localization on the carboxyl of central pyridine at the LUMO level. Thus, in isomer **2** configurations with 92% contribution (from the coefficient) and in isomer **2′** with two configurations with 99.4% contribution (from the coefficient), there is significant electron localization on the carboxyl of central pyridine. In isomer **3**, there is significant electron localization on the carboxyl of central pyridine at the LUMO level. In isomer **3** configurations with 99.1% contribution (from the excitation coefficient), there is significant electron localization on the carboxyl of central pyridine. Although it has been observed that isomer **3** has slightly more metal contribution at the HOMO level than isomers **1**, **2**, and **2′**, it has been found that the HOMO−LUMO gap of isomer **3** is the highest and the HOMO−LUMO of isomer **1** is lowest among all the isomers. Because of this, isomer **1** is expected to be a better sensitizer than isomer **2**, which is predicted to be a better sensitizer than isomer **3**.

We now look at the higher-energy transitions in the isomers (Figure 3). It has been found that the higher-energy bands for all isomers are mainly from the LLCT, and this is more prominent in isomer **1**. For this isomer, the band centered at 2.84 eV corresponds to the intraligand transitions ($\pi \rightarrow \pi^*$) and is localized on the terpyridine ligands. Lower-energy bands for all isomers have mixed isothiocyanate metal-to-ligand contributions (i.e., MLCT (i.e., Ru d orbital to terpyridine) and LLCT (major transition is from isothiocyanate to terpyridine)). For the first band, the major contributing orbitals are HOMO and HOMO−1, while for the higher-energy bands, they are HOMO−2, HOMO−3, HOMO−4, HOMO−5, etc. for all isomers of BD. It is evident that the spectra in Figure 3, considering solvent effects, are in considerably better agreement with the experiment than the spectra computed in the gas phase, in terms of band positions and separations (see Supporting Information).[39] The inclusion of the solvent effect blue shifts λ_{max} with respect to the gas phase for all four isomers. In addition, the higher-energy ($\pi \rightarrow \pi^*$) bands were found to be more intense than the lower-energy bands for all isomers. Finally, we see that the main spectral features are reproduced well by theoretical calculations because the calculated spectra for all four isomers are only slightly red shifted compared to the experimental values (0.06−0.14 eV).

Conclusion

We have characterized the molecular and electronic structures of BD and its other linkage isomers by DFT methods including scalar relativistic ZORA. The optimized geometry and electronic structure of BD and its linkage isomers in their ground state have been presented, and the electronic structure of the singlet-excited state has been considered. It has been found that the DFT methods reproduce the experimental geometry much better with inclusion of SR-ZORA. From the detailed NBO analysis, we observe that the variations in the interactions between metal and terpyridine ligand are small for all four isomers, but prominent differences are observed in the interactions between metal and anionic ligands (i.e., thiocyanate and isothiocyanate) because of the alteration of the bonding atom from nitrogen to sulfur in the anionic ligand. The delocalizing interactions between both the organic and inorganic ligands and metal are higher in isomer **1** than in isomer **2,** which are higher than those in isomer **3**. Similarly, the most significant $\pi-\pi^*$ interactions also vary to a large extent from one isomer to other, and the order is same as above. TDDFT with inclusion of solvent effects and scalar relativistic ZORA reproduced the experimental results reasonably well. Frontier orbital analysis, performed for all isomers in solution, shows that HOMOs are predominantly composed by both Ru t_2g d orbitals and isothiocyanate or thiocyanate p orbitals. LUMOs of π character result from the antibonding contributions of terpyridine carbon 2p orbitals with considerable contribution from carboxylic groups.

The contributions from thiocyanate, isocyanate, and Ru metal to the HOMOs and contribution by terpyridine and carboxylic groups to LUMOs have an important role in the electron injection and regeneration performance, respectively, for dye-sensitized solar cells. Interestingly, the λ_{max} values, overall shape, and band separations of the spectrum of all isomers of BD are well reproduced only after the inclusion of solvent effects. The UV−vis spectra of isomers of BD are dominated by MLCT and LLCT in the visible region. The maximum wavelength (λ_{max}) of the low-energy MLCT + LLCT band of isomer **1** is red shifted compared to those of isomers **2** and **2′**, which are again red shifted compared to that of isomer **3**. The red shift of the longer wavelength band on going from the fully S-bonded isomer to fully N-bonded isomer is mainly caused by the stronger electron-donating power of the N-bonded isocyanate groups compared to the S-bonded thiocyanate, which increases the energy of the metal dπ orbitals. Moreover, it has been found from the study of molecular orbitals that the HOMO−LUMO gap of isomer **1** is lowest among all four isomers of BD. Theoretical calculations on the equatorial form of isomer **2 (**i.e., isomer **2′**) were also performed, and it was found to be energetically less stable by only 4.0 kcal/mol. Because the interconversion between isomers **2** and **2′** in solution is feasible, the experimental values of absorption spectra may have contribution from both **2** and **2′**. Finally, it can be concluded from this study that DFT/TDDFT with SR-ZORA and solvent included is capable of describing and distinguishing the spectral features of all four linkage isomers of BD with good quantitative agreement with the experimental data.

Acknowledgment. The authors thank the Director, IICT, and the Head, Inorganic Chemistry Division, IICT, for their constant encouragement in this work. G.K.C. thanks CSIR for a fellowship. The authors also thank Aisin Cosmos for partial funding of the project.

Supporting Information Available: Additional tables showing lowest-excitation energies, oscillator strengths, and dominant excitation character for the isomers. This material is available free of charge via the Internet at http://pubs.acs.org.

IC051851G